Three-dimensional illumination procedure for photodynamic therapy of dermatology

Xiao-ming Hu
Feng-juan Zhang
Fei Dong
Ya Zhou

SPIE.

Three-dimensional illumination procedure for photodynamic therapy of dermatology

Xiao-ming Hu,[a,*] **Feng-juan Zhang,**[a] **Fei Dong,**[b] **and Ya Zhou**[b]
[a]Beijing Institute of Technology, School of Life Science, Beijing 100081, China
[b]Beijing Institute of Technology, School of Optoelectronics, Beijing 100081, China

Abstract. Light dosimetry is an important parameter that affects the efficacy of photodynamic therapy (PDT). However, the irregular morphologies of lesions complicate lesion segmentation and light irradiance adjustment. Therefore, this study developed an illumination demo system comprising a camera, a digital projector, and a computing unit to solve these problems. A three-dimensional model of a lesion was reconstructed using the developed system. Hierarchical segmentation was achieved with the superpixel algorithm. The expected light dosimetry on the targeted lesion was achieved with the proposed illumination procedure. Accurate control and optimization of light delivery can improve the efficacy of PDT. © *The Authors. Published by SPIE under a Creative Commons Attribution 3.0 Unported License. Distribution or reproduction of this work in whole or in part requires full attribution of the original publication, including its DOI.* [DOI: 10.1117/1.JBO.19.9.098003]

1 Introduction

Photodynamic therapy (PDT) is a widely used dermatological treatment based on photodynamic reactions. A light-sensitive substance (i.e., photosensitizer) and a light source with a specific wavelength are used to kill targeted cells.[1–6] The safety and effectiveness of PDT primarily depend on irradiance, tissue oxygenation, light penetration, and local photosensitizer concentration.[7,8] The optimal light dosage for PDT should adequately yield lethal effects on the targeted tumor while minimizing damage on adjacent normal tissues.[9]

Common adverse effects of PDT include various degrees of pain and a burning sensation. Pain level increases with irradiance; however, the exact pain mechanism remains unclear.[10] Significant advances in light dosimetry studies of PDT have been obtained for *in vivo* propagation models, which correlate incident irradiance and physiological outcomes in biological materials.[11,12] However, light dosimetry is hardly controllable *in vivo* because of irregularly shaped lesions, segmentation difficulty in normal areas, the patient's movement during the treatment, and so on.

Various light sources can be used in PDT; these sources include lasers, solid-state light-emitting diodes (LEDs), gas discharge lamps, and incandescent filament lamps.[13] Conventional light delivery systems comprise a light source and a light diffuser to homogeneously illuminate target areas. Several types of light diffusers have been developed for topical use or for application in body cavities.[14–18] Despite their wide applications, diffusers exhibit limited abilities to adjust for complex surfaces.[14] Expanded beams or coupling fibers are used to deliver healing light and achieve a homogenous irradiance.[19,20] However, irradiance on lesions remains uneven following parallel-beam irradiation because of the curved surface of the human body. Integrating spheres have been introduced to improve

PDTs for skin diseases; the procedure principally focuses on evaluation instead of illumination.[21]

Image processing technology is often combined with PDT treatment and used in site-specific delivery and in the planning, assessment, and monitoring of PDT.[22–24] The introduction of imaging technologies can affect the current practice of PDT.[25] For dermatological PDT, image processing is used to segment lesions according to color information because skin diseases are often accompanied by external morphological changes. Proper segmentation can be used to guide light delivery systems.

This study proposes a three-step treatment procedure for PDT. First, the three-dimensional (3-D) morphology of an irregular lesion is reconstructed by structured light. This procedure allows the lesion to be divided into small patches that are assumed to be internally homogeneous. Then, the patches are classified by color and distance using the superpixel method. Finally, the desired light dosage on the target can be achieved by modifying the gray value of the pixels in the projector.

2 Materials and Methods

2.1 Demo System Design

A fast structured light system consisting of a camera (Nikon D50, Tokyo, Japan), a computing unit, and a projector (Sony VPL-DX11, Kōnan Minato, Tokyo, Japan) was implemented to obtain a 3-D model of a lesion in Fig. 1(a). The projector was used as the space modulator in 3-D reconstruction and then as the light source during treatment. The software process is shown in Fig. 1(b), and the flow path is introduced in the following sections.

2.2 Data Acquisition and 3-D Reconstruction

The system should be calibrated to determine the parameters of the camera and the projector [C&P, Fig. 1(b)], which included rotation and translation matrices (R, T) between them, as well as the calibration parameters of the lens in the C&P. A 3-D scanning of the head model was obtained by a series of structured

---

*Address all correspondence to: Xiao-ming Hu, E-mail: bithxm@bit.edu.cn
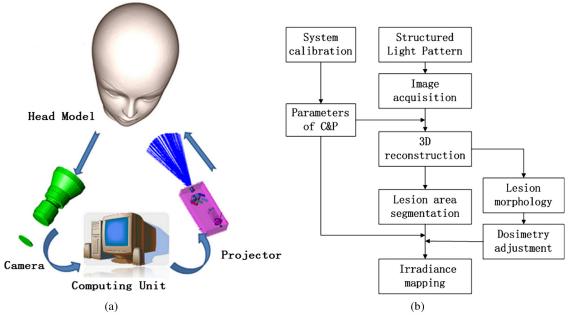
Fig. 1 (a) System configuration and (b) the software flow chart.

light patterns (e.g., gray code). Images were simultaneously taken from another angle. The coding and decoding of the gray code, which indicate the corresponding relation of the pixels on the image plane, is shown in Fig. 2. Each 3-D coordinate was indexed from its two-dimensional (2-D) coordinates on the camera image plane.[26] Hence, the texture of the 2-D image can be mapped onto the 3-D point cloud to form a 3-D model for observation and further operation.

2.3 Segmentation and Rating of Lesion

Setting the desired irradiance pixel by pixel remains difficult. Topical segmentation and classification in dermatology depend on the morphological changes of skin lesions, which vary with the disease. A superpixel clustering method was proposed for

segmentation and rating under different situations.[27] First, an original image was transformed to the LAB color space $[l_i, a_i, b_i]$, and parameter k was set to correspond to the number of areas that require treatment. The pixels were then clustered by their distances in the five-dimensional space along with their corresponding coordinates $[x_i, y_i]$ around the initial center pixel of $[x_k, y_k]$, as given by Eq. (1)

$$\begin{cases} d_{\text{lab}} = \sqrt{(l_k - l_i)^2 + (a_k - a_i)^2 + (b_k - b_i)^2} \\ d_{xy} = \sqrt{(x_k - x_i)^2 + (y_k - y_i)^2} \\ D_s = d_{\text{lab}} + \frac{m}{s} d_{xy} \end{cases}, \quad (1)$$

where s is the regular grid step and m weighs the relative importance between color similarity and spatial proximity.
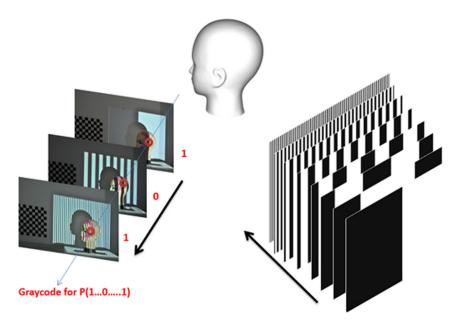

Fig. 2 Coding and decoding of the gray code.

Segmentation and rating can be conveniently performed for clustered images.

2.4 *Light Delivery*

Some of the main concerns related to using projectors as illumination sources include irradiation alignment and incident angle calculation; the latter was essential for targeted and homogeneous irradiances in the lesion. A simplified illumination model is demonstrated in Fig. 3. $O_{c1}X_{c1}Y_{c1}Z_{c1}$ and $O_pX_pY_pZ_p$ represent the coordinates of the camera and projector, respectively, P_c is the image plane, and P_g is the projector plane. Given the known 3-D coordinates of the skin diseases, the mapping relation from the image plane coordinate $[x_c, y_c, z_c]$ to the projector coordinates $[x_p, y_p, z_p]$ can be described as follows:

$$[x_p, y_p, z_p]^T = F[R([x_c, y_c, z_c]^T + T)], \tag{2}$$

where F is the map function of the pixels from the camera plane to the projector plane. The maximum irradiance received by the disease voxel from a projector pixel can be estimated as follows:

$$E_{max} = \frac{P\eta \cos\theta(\cos\gamma)^4}{HL\beta^2}, \tag{3}$$

where P is the luminous power of the lamp, η is the utilization rate of light energy, $H * L$ is the projector resolution, θ is the angle between the incident ray O_pP and the surface normal n of the disease, γ is the angle between O_pP and the optical axis of the projector, and β is the zoom factor of the projector, which is approximated by Eq. (4)

$$\beta = Z_p/f_p, \tag{4}$$

where Z_p is the distance from the target voxel in the projector coordinates and f_p is the projector focal length that can be achieved during calibration.

The target irradiance for a practical voxel can be achieved by modifying the gray value of the projection image. For example, the pulse width of modulation in a digital light projector was linearly correlated with the irradiance. The gray value of the corresponding pixel was then calculated upon setting the desired irradiance. An example of a reverse projection image is shown in Fig. 4.
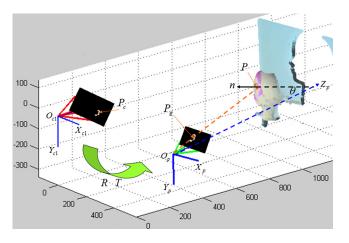

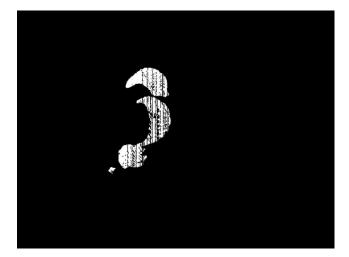**Fig. 3** A simplified illumination model.

Fig. 4 An example of reverse projection image.

3 Experimental Results

3.1 *3-D Reconstruction and Evaluation*

The 3-D reconstruction and evaluation with a resolution of < 1 mm in the x, y, and z axes is illustrated in Fig. 5. The head model was reconstructed by a 3-D scanner (3D CaMega, Boweihengxin Ltd., Beijing, China) for reference. Figure 5(a) shows $\sim 777,117$ and 345,170 vertices that were obtained from our reconstruction in the left (in brown) and right (in black) with abbreviations of 3-D Sca. and 3-D Rec., respectively. The 3-D point clouds were evaluated by MeshLab. Figure 5(b) shows that the Hausdorff distances were < 1 mm in most of the vertices and that the gross errors were almost in the boundary with no points in our 3-D reconstruction because of the shadow.

3.2 *Segmentation Results*

The clustering results for different k and skin diseases are revealed in Figs. 6 and 7, respectively. The original image of Fig. 6 is a phantom of a port-wine stain (PWS), where the red region represents the lesion. The number of segmentations increased with k. This result indicates that segmentation is a flexible and convenient clustering method because the threshold or initial conditions need not be set. Zhang[27,28] demonstrated that segmentation can be evaluated by various techniques and that segmentation applications can be considered during selection. Common empirical methods were used to test the segmentation quality in all four experiment groups (Table 1).[29,30] UM is the intraregion uniformity measurement, GC is the gray-level contrast between regions, VC is the interregion vergence contrast, MI(k) is the rate of pixels that should be segmented when they are not with the proposed algorithm, and MII(k) is the rate of pixels that should not be segmented. MI(k) and MII(k) were obtained by comparing the experimental results with the theoretical results by manual specification.

The severities of skin disease are often hierarchical. For instance, the severity of PWS is graded in six levels. The head model was painted with common colors (e.g., purple, dark violet, light red, and dark red) for demonstration.[31] The areas with different colors were clustered separately (Fig. 8). The expected light dosimetry can be mapped from the camera plane to the projector plane as described in Sec. 2.4.
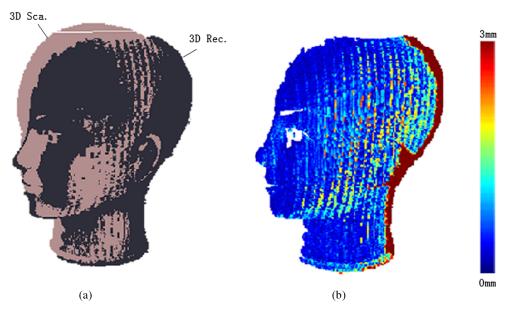
Fig. 5 Three-dimensional (3-D) reconstruction results compared with the data from a 3-D scanner.
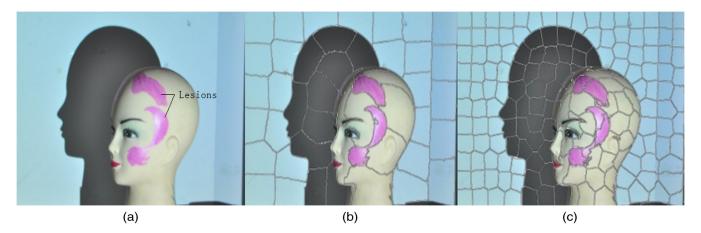

Fig. 6 Original image (a) with clustering results when k is 50 (b) and 200 (c).

Fig. 7 Clustering and segmentation results for some dermatological diseases: (a) herpes zoster, (b) hemangioma cutis, (c) tinea corporis, and (d) leucoderma.

3.3 Illumination Results

Given the 3-D reconstruction of the lesion, we can estimate the surface normal at each patch by its surrounding neighbors and their gravity. The cosines of the incident angles of each patch on the surface with five discrete levels for simplicity are shown in Fig. 9. Only one third of the incident rays are nearly vertical to the surface. Thus, even illumination can hardly be obtained on a curved lesion illuminated directly by a flat source.

Internal points can be regarded as the interpolation of boundary points. Thus, the difference between the lesion and the reverse projection can be assessed by the degree of boundary

Table 1 Evaluation of the segmentation by different properties.

	Uniformity measurement	Gray-level contrast	Vergence contrast	MI(k)[a]	MII(k)[b]
Image (a)	0.63	0.74	0.64	2.6%	1.3%
Image (b)	0.24	0.88	0.79	1.7%	0.3%
Image (c)	0.57	0.67	0.72	5.0%	4.9%
Image (d)	0.46	0.52	0.60	2.3%	3.1%

[a]MI(k) is the rate of pixels that should be segmented when they are rejected by the proposed algorithm.
[b]MII(k) is the rate of pixels that should not be segmented when they are accepted by the proposed algorithm.
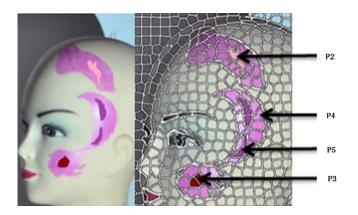

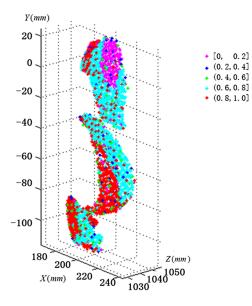**Fig. 8** Grading sample for port-wine stain.

Fig. 9 Cosines of incident angles for various lesions.

matching. The red region in the left of Fig. 6 represents the targeted lesion. The highlighted areas in Fig. 10 were illuminated to verify the correctness of the reverse projection or treatment illumination. The incidence was well targeted, and the normal areas were protected without any additional work. The borders were matched on the lesion, which verified the accuracy of the segmentation and reconstruction.

4 Discussion

Considering the limitations of the experimental conditions and clinical trials, we verified the following parameters:

4.1 Spectrum of Light Source

Monochromatic light is the optimal choice in PDT, but LED and other nonlaser light sources are also widely used. The depth of light penetration into the tissue is related to the light spectrum. Although projectors are often based on lamps, laser and LED light engines are used in high-brightness projectors. LED or laser projectors can be used with the right color channel, or the light engine can be modified with a correct laser source. Two or three color channels can also be combined by different laser types, which are beneficial in simultaneously treating diseases at different depths.

4.2 Projector Irradiance

The power density required for PDTs is typically 70 to 100 mW/cm^2. Light sources with power outputs of 5 to 10 W are suitable for most treatments; several modules are also available. For example, Luminus developed an LED chip PT-120 for a TI DLP® light engine with 5400 lumen at 525 nm. Laser light engines possess a green laser module DSG265 that provides a digital projection of up to 35 W. For the modulator in the projector, the DMD9500 datasheet exhibits a threshold density of up to 20 W/cm^2 in the visible spectrum. This threshold density corresponds to 48 W for the device, which meets PDT requirements. The proposed digital illumination procedure allowed modulation either by modulating the light source or by modifying the gray value of the pixel.

4.3 Lesion Identification

The head model painted with different colors verified the correctness of the reverse projection. Although color is a characteristic of lesions, its identification requires professional clinical diagnosis. 3-D reconstruction and segmentation provided a convenient control for treatment, for example, by making the treatment area larger than the lesion-defined area, reserving a specific untreated area, or illuminating different areas at various levels.

4.4 Optical Parameters of Human Skin

Optical parameters (e.g., specular reflection, absorption coefficient, scattering coefficient, photosensitizer absorption, and the index of refraction) vary from person to person. These parameters are related with thermal damage, pain, and treatment evaluation; hence, optimal protocols in the site are highly difficult. All parameters should be achieved and used to calibrate the gray value of the illumination image for the treatment to provide an accurate and ideal PDT. Protocols of different wavelengths or modes of light modulation can be simultaneously assessed on the same patient to understand the mechanism of PDT.

4.5 Patient Movement During the Treatment

Patient movement during PDT is too difficult to avoid because of the treatment time and pain. PDT is tiring because it takes ~30 min per session. Moreover, the procedure can be very excruciating due to various levels of pain and burning sensations.

Fig. 10 Reverse projection results viewed from different angles.

The proposed procedure allows 3-D reconstruction of the lesion at timed intervals as prescribed by a doctor. Then, the result can be registered and aligned with the original 3-D model. Thus, each treatment dosimetry can be not only reserved but also statistically analyzed and compared.

5 Conclusion

The 3-D reconstruction and the hierarchical segmentation of the lesion were introduced into PDT for dermatological treatment. Parameters such as distance from the light source to the target treatment voxel, angle between the normal vectors of lesion patch and the incident light, lesion level, and so on can be achieved and classified. These parameters can yield a controllable light dosimetry for complex lesions on curved surfaces, and specific treatment procedures can be performed with less manual labor by doctors.

Moreover, 3-D lesion reconstruction can also help plan PDT treatments and evaluate the outcome of different treatment sessions to potentially standardize light delivery.

References

1. J. A. Leman and C. A. Morton, "Photodynamic therapy: applications in dermatology," *Expert Opin. Biol. Ther.* **2**(1), 45–53 (2002).
2. I. J. MacDonald and T. J. Dougherty, "Basic principles of photodynamic therapy," *J. Porphyr. Phthalocyanines* **5**(2), 105–129 (2001).
3. D. Dolmans, D. Fukumura, and R. K. Jain, "Photodynamic therapy for cancer," *Nat. Rev. Cancer* **3**(5), 380–387 (2003).
4. J. S. McCaughan, "Photodynamic therapy—a review," *Drugs Aging* **15**(1), 49–68 (1999).
5. T. J. Dougherty, "An update on photodynamic therapy applications," *J. Clin. Laser Med. Surg.* **20**(1), 3–7 (2002).
6. P. Babilas et al., "Photodynamic therapy in dermatology: state-of-the-art," *Photodermatol. Photoimmunol. Photomed.* **26**(3), 118–132 (2010).
7. R. Bays et al., "Three-dimensional optical phantom and its application in photodynamic therapy," *Lasers Surg. Med.* **21**(3), 227–234 (1997).
8. L. M. Vesselov, W. Whittington, and L. Lilge, "Performance evaluation of cylindrical fiber optic light diffusers for bio-medical applications," *Lasers Surg. Med.* **34**(4), 348–351 (2004).
9. S. B. Brown, "The role of light in the treatment of non-melanoma skin cancer using methyl aminolevulinate," *J. Dermatol. Treat.* **14**(Suppl. 3), 11–14 (2003).
10. Y. N. Chaves et al., "Pain in photodynamic therapy: mechanism of action and management strategies," *An. Bras. Dermatol.* **87**(4), 521–529 (2012)..
11. T. C. Zhu, J. C. Finlay, and S. M. Hahn, "Determination of the distribution of light, optical properties, drug concentration, and tissue oxygenation in-vivo in human prostate during motexafin lutetium-mediated photodynamic therapy," *J. Photochem. Photobiol. B.* **79**(3), 231–241 (2005).
12. T. C. Zhu, J. C. Finlay, and S. M. Hahn, "Optimization of light dosimetry for photodynamic therapy of Barrett's esophagus: efficacy vs. incidence of stricture after treatment," *Gastrointest. Endosc.* **61**(1), 13–18 (2005).
13. L. Brancaleon and H. Moseley, "Laser and non-laser light sources for photodynamic therapy," *Lasers Med. Sci.* **17**(3), 173–186 (2002).
14. B. Selm et al., "Novel flexible light diffuser and irradiation properties for photodynamic therapy," *J. Biomed. Opt.* **12**(3), 034024 (2007).
15. V. G. Schweitzer, "Photofrin-mediated photodynamic therapy for treatment of aggressive head and neck non melanomatous skin tumors in elderly patients," *Laryngoscope* **111**(6), 1091–1098 (2001).
16. L. Guyon et al., "Development of a new illumination procedure for photodynamic therapy of the abdominal cavity," *J. Biomed. Opt.* **17**(3), 038001 (2012).
17. C. Canavesi et al., "Design of illumination devices for delivery of photodynamic therapy in the oral cavity," *Appl. Opt.* **50**(16), 2322–2325 (2011).
18. S. J. Madsen et al., "Development of a novel in dwelling balloon applicator for optimizing light delivery in photodynamic therapy," *Lasers Surg. Med.* **29**(5), 406–412 (2001).
19. H. van den Bergh, "On the evolution of some endoscopic light delivery systems for photodynamic therapy," *Endoscopy* **30**(4), 392–407 (1998).
20. J. Zubia and J. Arrue, "Plastic optical fibers: an introduction to their technological processes and applications," *Opt. Fiber Technol.* **7**(2), 101–140 (2001).
21. D. L. Glennie et al., "Integrating spheres for improved skin photodynamic therapy," *J. Biomed. Opt.* **15**(5), 058001 (2010).
22. N. S. Soukos et al., "Epidermal growth factor receptor-targeted immunophotodiagnosis and photoimmunotherapy of oral precancer *in vivo*," *Cancer Res.* **61**(11), 4490–4496 (2001).
23. Y. E. Koo et al., "Photonic explorers based on multifunctional nanoplatforms for biosensing and photodynamic therapy," *Appl. Opt.* **46**(10), 1924–1930 (2007).
24. J. R. McCarthy and R. Weissleder, "Multifunctional magnetic nanoparticles for targeted imaging and therapy," *Adv. Drug Deliv. Rev.* **60**(11), 1241–1251 (2008).
25. J. P. Celli et al., "Imaging and photodynamic therapy: mechanisms, monitoring, and optimization," *Chem. Rev.* **110**(5), 2795–2838 (2010).

26. D. Moreno and G. Taubin, "Simple, accurate, and robust projector-camera calibration," in *Second Int. Conf. on 3D Imaging, Modeling, Processing, Visualization and Transmission*, pp. 464–471, IEEE (2012).
27. R. Achanta et al., "SLIC superpixels compared to state-of-the-art superpixel methods," *IEEE Trans. Pattern Anal.* **34**(11), 2274–2282 (2012).
28. H. Zhang, J. E. Fritts, and S. A. Goldman, "Image segmentation evaluation: a survey of unsupervised methods," *Comput. Vis. Image Underst.* **110**(2), 260–280 (2008).
29. M. D. Levine and A. M. Nazif, "Dynamic measurement of computer generated image segmentations," *IEEE Trans. Pattern Anal.* **7**(2), 155–164 (1985).
30. W. A. Yasnoff, J. K. Mui, and J. W. Bacus, "Error measures for scene segmentation," *Pattern Recognit.* **9**(4), 217–231 (1977).
31. H. Cheng et al., "Chromatism of port-wine stains before and after photodynamic therapy," *Chin. J. Laser Med. Surg.* **19**(3), 137–141 (2010).

Xiao-ming Hu received his BS degree in physical electronics from Beijing Institute of Technology (BIT) in 2001 and received his PhD degree in optical engineering from BIT in 2006. He has been working at the School of Life Science in BIT since then. His research interests include biomedical photonics, piezosurgery, and optical detection in microfluidics.

Feng-juan Zhang received her BS degree from School of Automatic, Zhengzhou University in 2013 and is a candidate for the M S degree in biomedical engineering of BIT. Her research interests include biomedical photonics and three-dimensional (3-D) reconstruction.

Fei Dong received his BS degree in mechanics from Wuhan University in 2010 and his MS degree in optical engineering from BIT in 2014. His research interests include machine vision and 3-D reconstruction.

Ya Zhou received her PhD degree in optical engineering from BIT in 2000. After two years of postdoctoral research at School of Earth and Space Sciences, Peking University, she joined BIT as an associate professor in 2002. Her research interests include biometrics technology, medical image analysis, and computer vision.